Optimization of Thermal Control Design for Aerial Reflective Opto-Mechanical Structure

Yun Zhou * , Huilin Wang , Xiaocun Jiang , Xiaozhou Zuo , Ming Chen

Posted Date: 29 December 2023

doi: 10.20944/preprints202312.2319.v1

Keywords: Opto-mechanical structure; Optimized thermal control; Temperature uniformity; Image quality

Article

Optimization of Thermal Control Design for Aerial Reflective Opto-Mechanical Structure

Zhou Yun, Wang Huilin, Jiang Xiaocun, Zuo Xiaozhou and Chen Ming

Xi'an Institute of Applied Optics
* Correspondence: zy9798@163.com

Abstract: To improve the adaptability of aerial reflective opto-mechanical structures to low-temperature environments, an optimized thermal control design is proposed. Firstly, the relationship between conventional heating methods and axial/radial temperature differences of mirrors with different shapes is analyzed. Based on heat transfer analyses, it is pointed out that optimized thermal control design is necessary to ensure the temperature uniformity of the fused silica mirror and take into account the temperature level when working in low temperature environments. A thermal control scheme based on temperature negative feedback variable power zone heating is proposed for the characteristics of aerial electro-optics systems. Using the thermal control scheme at low temperatures ensures that the average temperature of the mirror fluctuates slowly and slightly around 20℃. At the same time, the temperature differences within a mirror and between the primary mirror and the secondary mirror can be controlled within 5℃. Thereby, satisfactory image quality is obtained.

Keywords: opto-mechanical structure; optimized thermal control; temperature uniformity; image quality

1. Introduction

To obtain clear image, spacecraft and aircraft are equipped with electro-optics systems (EO) [1,2]. Generally, EO mainly includes electronic units, opto-mechanical structure, and imaging sensors, which are mounted inside the cabin. For large EO, the opto-mechanical structure is often designed as a reflective type, and the main optical components include primary mirror and secondary mirror [3,4].

To improve the ability to clearly image distant targets, it is necessary to have a larger aperture for the primary mirror and secondary mirror, while ensuring minimal wavefront error (WFE) on the reflective surface [5]. WFE is impacted by manufacturing and assembly technology, and also varies with environmental factors [6,7]. Among various environmental factors, the influence of temperature is enormous. When the temperature changes, the curvatures of primary mirror and secondary mirror deviate from the design values due to the thermal expansion or contraction. More importantly, due to the non-uniform temperature distribution of the mirror, the displacement caused by temperature changes at each point is also different. Therefore, in addition to uniform expansion or contraction, irregular deformation occurs. The complex deformation brings optical aberrations which are difficult to eliminate, thereby reducing image quality.

Optical aberrations analysis can be completed by fitting the distorted surface using Zernike polynomials. Reference [8] analyzed the aberration and image quality under given temperature conditions. Based on the simulation results, the temperature level and allowable temperature differences that the opto-mechanical structure need to maintain were provided. In practice, the temperature distribution is influenced by various heat transfer modes, making it difficult to pre determine [9]. In addition, simulation techniques need to be improved to comprehensively and accurately evaluate aberrations and image quality [10,11]. Therefore, in product design, it is common practice, to directly prescribe the working temperature of the opto-mechanical structure, based on

 doi:10.20944/preprints202312.2319.v1

task requirements and the difficulty of thermal control, and considering previous experience, including the average temperature of primary mirror and secondary mirror, the temperature difference between them, and their own temperature uniformity. Based on the temperature distribution, the performance of the opto-mechanical structure and the image quality of the EO can be guaranteed. For the spacecraft opto-mechanical structure, temperature uniformity is easily satisfied since the heat transfer modes are conduction and radiation only. For aerial opto-mechanical structure, however, temperature is also affected by complex convection, which makes uniformity more difficult. Therefore, the axial/radial temperature differences within the mirrors, as well as the temperature difference between primary mirror and secondary mirror, are generally limited to 5℃, while the average temperature fluctuates slightly around 20℃ [2,12].

Due to the significant temperature changes in the environment where the EO operates, thermal control design must be carried out to ensure that the opto-mechanical structure, especially primary mirror and secondary mirror, meets the temperature prescriptions during the working cycle. When the mirror is made of silicon carbide (SiC), due to its large thermal conductivity, temperature uniformity is easily satisfied, and therefore a large heating power can be used to ensure the average temperature of the mirror. The fused silica mirror, while offering great merits, such as matured and low-cost manufacturing and hence wide usage, presents also great challenge: a small thermal conductivity, which makes temperature uniformity difficult. It is necessary to reduce the heating power to ensure temperature uniformity, but this will reduce the temperature rise ability.

To guarantee the temperature uniformity of the fused silica mirror, this article analyze the relationship between conventional heating method and axial/radial temperature differences, and an optimized thermal control design based on temperature negative feedback variable power zonal heating is proposed. Through this thermal control technology, the axial/radial temperature differences can be controlled within 5℃; At the same time, it keeps a balance between heating power and heat losses, ensuring that the temperature is at an appropriate level during the working cycle, thereby guaranteeing good image quality of EO.

2. Typical Aerial Opto-Mechanical Structure and Its Heat Transfer

A typical aerial opto-mechanical structure is shown in Figure 1. The primary mirror and secondary mirror are mounted on the primary mirror holder and secondary mirror holder respectively, and they are connected through the optic bench and secondary mirror bracket to form the main body of the reflective opto-mechanical structure. The opto-mechanical structure is connected to the shell of the EO through supporting components, and is surrounded by a cabin formed by the shell and the optical window, which is usually cylindrical or spherical.

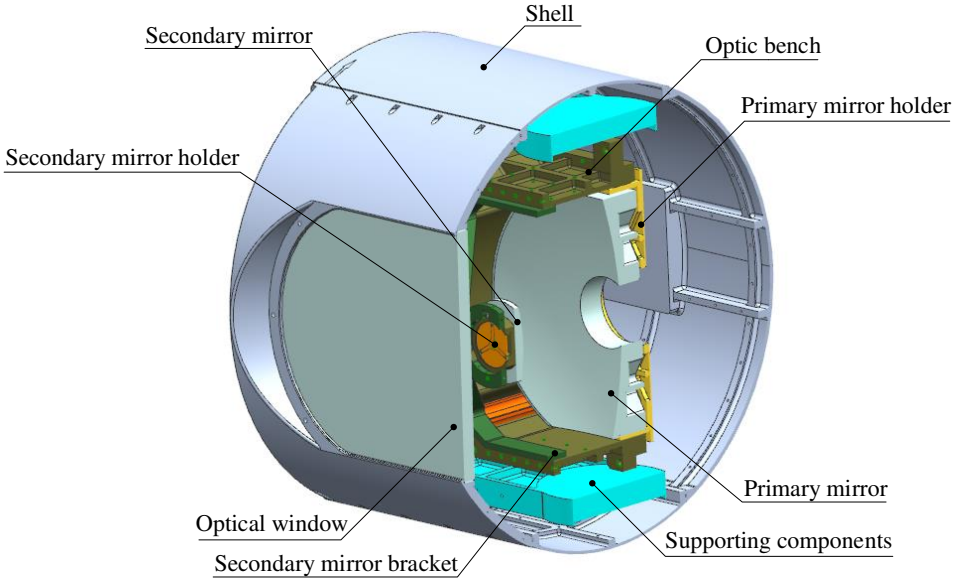

 doi:10.20944/preprints202312.2319.v1

Figure 1. Structure of reflective opto-mechanical structure.

As the flight altitude and endurance of the aircraft increase, the opto-mechanical structure will undergo long-term heat exchange with low-temperature environments, resulting in a decrease in its own temperature. Firstly, conduction occurs between the opto-mechanical structure and the supporting components, and the heat is ultimately transmitted to the shell. The primary mirror and secondary mirror are bonded to the primary mirror holder and secondary mirror holder through silicone rubber, which is insulative and has a small bonding area. Therefore, the heat losses of primary mirror and secondary mirror by conduction are very small. For optic bench and support components with contact surface temperatures of T_{ob} and T_{sc}, the heat rate by conduction is calculated according to formula (1):

$$Q_{\text{cond}}^{\text{ca}} = A_{\text{ca}} \frac{T_{\text{ob}} - T_{\text{sc}}}{R_{\text{cont}}} \tag{1}$$

In formula (1), A_{ca} is the contact area between the two, and R_{cont} is the contact thermal resistance. Generally, A_{ca} is small while R_{cont} is large.

Secondly, the cabin is filled with air and undergoes heat exchange with the opto- mechanical structure through convection, transferring heat to the shell and the optical window, and ultimately diffusing to the external environment. Taking a typical aerial primary mirror as an example, the reflective surface is approximated as a plane, and the normal direction is perpendicular to the direction of gravity. The characteristic size (usually aperture) is L=300mm, the temperature of the reflective surface T_{pm}=293K, and the temperature of the air T_a=213K. That is, after working for a period of time, the temperature of the interior air of the cabin is consistent with the external environment temperature (this phenomenon is consistent with reality). The air flow inside the cabin is in free convection, with Raleigh number Ra_x:

$$Ra_x = \frac{2g\left(T_{\text{pm}} - T_{\text{a}}\right)x^3}{\left(T_{\text{pm}} + T_{\text{a}}\right)\nu^2} Pr = \frac{13.72\left(T_{\text{pm}} - T_{\text{a}}\right)x^3}{\left(T_{\text{pm}} + T_{\text{a}}\right)\nu^2},\ x \in [0, L] \tag{2}$$

In formula (2), the acceleration of gravity g=9.8m/s^2, the Prandtl number of air Pr=0.7, and its kinematic viscosity ν calculated according to the $(T_{pm}+T_a)/2$ condition, it is 11.71×10^{-6}m^2/s. Formula (2) calculates $Ra_x \le Ra_L$=4.3×10^8 ≤ 10^9, meaning that the Raleigh number at any position on the reflective surface does not exceed the critical value, therefore it is laminar free convection [13]. Correspondingly, calculate the average convection coefficient $\bar{h}$ of the reflective surface according to formula (3)

$$\bar{h} = \frac{1}{L}\int_0^L h_x \mathrm{d}x = \frac{1}{L}\int_0^L \left[\frac{g\left(T_{\text{m}} - T_{\text{a}}\right)x^3}{2\left(T_{\text{m}} + T_{\text{a}}\right)\nu^2}\right]^{\frac{1}{4}} \cdot \frac{k}{x} \cdot f\left(Pr\right)\mathrm{d}x \tag{3}$$

Where k is the thermal conductivity of the air at a temperature of $(T_{pm}+T_a)/2$, which is 22.54×10^{-3}W/(m·K); $f(Pr)$ is a function of the Prandtl number:

$$f\left(Pr\right) = \frac{0.75Pr^{1/2}}{\left(0.609 + 1.221Pr^{1/2} + 1.238Pr\right)^{1/4}} \tag{4}$$

By combining formulas (3) and (4), $\bar{h}$ of the reflective surface can be calculated to be approximately 5.57W/(m^2·K). It should be pointed out that there are other criteria for deciding whether the heat transfer is laminar or turbulence. There are also different calculation methods for $\bar{h}$, but the results are not significantly different.

The third heat transfer mode of opto-mechanical structure is radiation. Assuming that all surfaces are diffuse gray surfaces in the analysis, their emissivity ε equals to absorptivity α. ε is

 doi:10.20944/preprints202312.2319.v1

directionally independent, and can be regarded as a constant within the operating temperature range of EO. For the opto-mechanical structure, it is located within the envelope formed by the shell and the optical window, its emissivity is ε_{os}. The absolute temperature of the opto-mechanical structure and envelope are T_{os} and T_{en} respectively. Denote the radiation area of the opto-mechanical structure is A_{os}, then the radiation power Q_{rad}^{os} from the opto-mechanical structure to the envelope can be estimated as [14]:

$$Q_{rad}^{os} = A_{os}\varepsilon_{os}\sigma\left(T_{os}^4 - T_{en}^4\right) \tag{5}$$

In formula (5), σ=5.67×10^{-8}W (m^2·K^4) is the Stefan-Boltzmann constant. Obviously, the higher the value of T_{en}, the less heat the opto-mechanical structure loses through radiation; When $T_{os} < T_{en}$, $Q_{rad}^{os} < 0$, it means that the opto-mechanical structure is heated. In order to obtain accurate results, the radiation of components such as the primary mirror, secondary mirror, and optic bench must be calculated more elaborately, often using numerical methods. However, formula (5) can be used to qualitatively analyze the trend of radiation heat transfer.

3. Analysis of Temperature Uniformity and Optimization of Thermal Control

The analysis in the second section shows that the heat losses of the opto-mechanical structure is mainly through convection and radiation. Although electronic units and imaging sensors generate heat during operation, it is not sufficient to compensate for the heat losses of the opto-mechanical structure. Without additional heat input, the temperature of the opto-mechanical structure will ultimately match the ambient temperature. By then, the image quality may become very poor. Figure 2 shows the image of observing the resolution test chart of a certain EO after being stored at -40℃ for 6 hours. At this point, the temperature of the opto-mechanical structure is about -35℃, and clear imaging is impossible. Therefore, it is necessary to heat up the opto-mechanical structure, especially the primary mirror and secondary mirror, to ensure the image quality of EO.

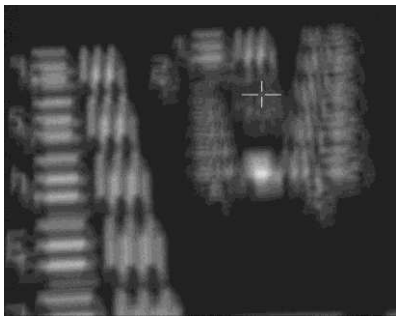

Figure 2. Image Quality in Low Temperature Environment.

The conventional heating method for the primary mirror is to arrange a heating zone on its back [16]. The heat starts from the primary mirror holder and reaches the back of the primary mirror through radiation and conduction, and continues to transmit axially to the reflective surface. This brings about axial/radial temperature differences. The following analyzes the relationship between temperature uniformity and heating power for reflective faces of different shapes and materials, and proposes an optimized thermal control with the goal of reducing temperature gradient.

Take a spherical reflective face as an example, as shown in Figure 3. Denote the curvature radius as R, the aperture D, the center thickness h, and there is a hole with a radius of r_0 in the center of the mirror. The thermal conductivity of the mirror is k.

Preprints (www.preprints.org) | NOT PEER-REVIEWED | Posted: 29 December 2023 doi:10.20944/preprints202312.2319.v1

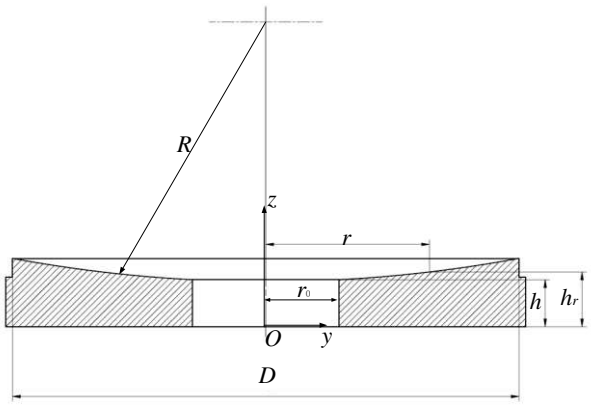

Figure 3. Spherical Mirror.

Obviously, on the reflective surface, at a radial coordinate $r(0\le r\le D/2)$, the distance h_r from the back is:

$$h_r = h + R - \sqrt{R^2 - r^2} \tag{6}$$

When the back of the mirror is heated, the vast majority of heat is transferred from the back to the reflective surface through conduction. The heat transfer rate q_{cond} per unit area is shown in formula (7):

$$q_{\text{cond}} = -k\frac{\mathrm{d}T}{\mathrm{d}z} \tag{7}$$

Assuming a uniform temperature distribution T_b on the back, under steady-state conditions, the temperature T_r of the reflective surface at the radial coordinate r can be calculated using formula (6) and formula (7):

$$q_{\text{cond}} = k\frac{T_{\text{b}} - T_r}{h_r} \Rightarrow T_r = T_{\mathbf{b}} - \frac{q_{\text{cond}}}{k}\left(h + R - \sqrt{R^2 - r^2}\right) \tag{8}$$

Therefore, the maximum axial temperature difference ΔT_{ax} appears at the outer edge of the reflective surface:

$$\Delta T_{\text{ax}} = \frac{q_{\text{cond}}}{k}\left(h + R - \sqrt{R^2 - \frac{D^2}{4}}\right) \tag{9}$$

The maximum radial temperature difference ΔT_{rad} caused by conduction can also be obtained through formula (8):

$$\Delta T_{\text{rad}} = \frac{q_{\text{cond}}}{k}\left(\sqrt{R^2 - r_0^2} - \sqrt{R^2 - \frac{D^2}{4}}\right) \tag{10}$$

Therefore, based on the temperature difference threshold, combined with formulas (9) and (10), the maximum allowable heating power can be estimated. Similarly, when the reflective surface is parabolic, T_r, ΔT_{ax}, ΔT_{rad} are respectively:

$$T_r = T_{\text{b}} - \frac{q_{\text{cond}}}{k}\left(h + \frac{1}{2}cr^2\right) \tag{11}$$

$$\Delta T_{\text{ax}} = \frac{q_{\text{cond}}}{k}\left(h + \frac{1}{8}cD^2\right) \tag{12}$$

Preprints (www.preprints.org) | NOT PEER-REVIEWED | Posted: 29 December 2023 doi:10.20944/preprints202312.2319.v1

$$\Delta T_{\text{rad}} = \frac{1}{2} c \frac{q_{\text{cond}}}{k} \left(\frac{1}{4} D^2 - r_0^2 \right) \tag{13}$$

In formulas (11) to (13), c represents the curvature at the center of the reflective surface, and the meanings of other symbols are consistent with those of spherical mirrors. Similarly, the temperature distribution of other types of reflective surfaces can be analyzed.

From formulas (9), (10), (12), and (13), it can be inferred that, under the premise of consistent geometric size and temperature uniformity requirements, the larger the value of k, the greater the allowable heating power. For mirrors made of SiC material, k_{SiC} exceeds 100W/(m·K), so a large amount of power can be applied to the back for heating, allowing the mirror to have sufficient temperature rise capacity, while the temperature gradient is controlled within the specified range. For fused silica mirrors, k_{fs} is barely 1/100 of k_{SiC}, so the back heating power must be well controlled to avoid large temperature gradient. In addition, it is necessary to consider the convection of the reflective surface in reality, and it is difficult to ensure uniform distribution of q_{cond} on the entire back surface. These factors will increase the temperature gradient on the mirror. Therefore, in reality, the allowable maximum heating power is smaller than the estimated value.

Consider a fused silica primary mirror with a spherical reflective surface, k_{fs}=1.37 W/(m·K) (see Table 3.12 of reference [15]), R=600mm，D=220mm，h=20mm， r_0=35mm. When the maximum allowable axial/radial temperature differences are 5°C, q_{cond}=227 W/m^2, a maximum heating power of approximately 7.8W on the back can be applied. As a comparison, calculate the maximum allowable heating power of the SiC mirror. k_{SiC} is about 150W/(m·K) (see Table 3.13 of reference [15]), and the corresponding back heating power can be increased to 849W; Even if the axial/radial temperature differences are limited to 0.5°C, the back heating power can still maintain 85W. On the other hand, according to formula (3), when the mirror and air temperatures are 20°C and -60°C respectively, the rate of heat loss is about 16.4W. This means that when EO operates at low temperatures for a long time, in order to maintain the temperature level while ensuring temperature uniformity, mirrors of SiC material need heating on the back only [4,16]; For fused silica mirrors, however, in addition to back heating, more optimized heating measures must also be introduced to maintain temperature level.

One optimization measure is to arrange thermal control devices on the shell, including passive insulation and active heating, as shown in Figure 4. The insulation layer with a small thermal conductivity is bonded on the interior surface of the shell, reducing the rate of heat loss from the inside of EO to the external environment; The heating cover, a metal sheet made of large thermal conductivity, is connected to the shell. The heating cover is attached with a heating film, and the heat generated by the latter is evenly distributed on the heating cover, heating the opto-mechanical structure in a radiative manner. The temperature sensor is bonded on the back of the heating cover. In addition, considering that convection inside the cabin leads to high temperatures in the upper part and low temperatures in the lower part, active heating is divided into multiple zones, each zone having independent power control, as shown in Figure 5. The heating power of Region 1 and Region 2 is lower than that of Region 3 and Region 4. When the cabin rotates, Region 1 and Region 2 will turn down, and Region 3 and Region 4 will turn up, the heating power of the corresponding area will be increased or decreased accordingly.

 doi:10.20944/preprints202312.2319.v1

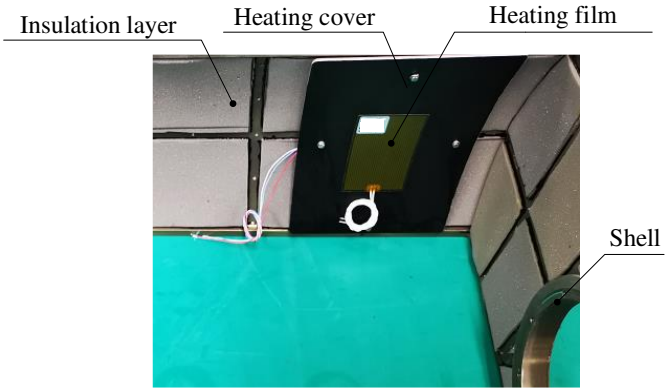

Figure 4. Shell Thermal Control.

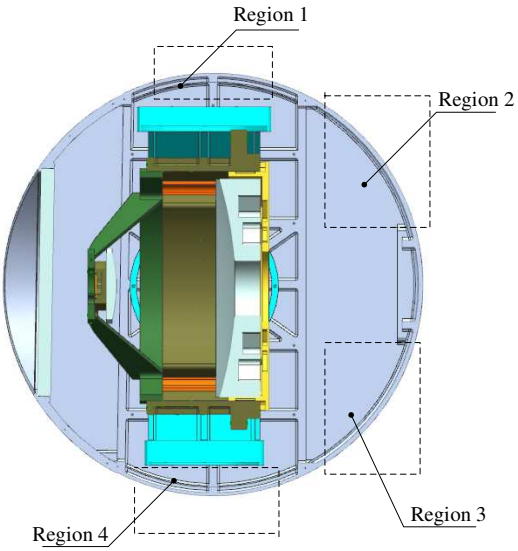

Figure 5. Shell Zonal thermal control.

From Figure 5, it can be observed that the view factor of the shell with respect to the primary mirror and secondary mirror is relatively small, indicating that the ratio of the radiation energy leaving shell that is intercepted by the primary mirror and secondary mirror is small. If a heating zone is set in front of the primary mirror (such as the front part of the shell, or the front part of the optic bench [8,16]), although the view factor can be increased, it will cause uneven air temperature in front of the primary mirror, leading to fluctuations of the index of refraction and reducing image quality. To improve heating efficiency and ensure image quality, heating films are arranged in the circumference of the primary mirror holder, not protruding beyond the front edge of the primary mirror along the axis direction, as shown in Figure 6. Like shell heating, the circumferential heating of the primary mirror holder is also divided into multiple zones, and sensors are arranged on the back and outer edge of the mirror to measure temperature. Considering the wide range of environmental temperature changes in practical use, the heating power of each zone is independently controlled through temperature negative feedback to obtain dynamic temperature adjustment and meet the thermal control needs within the working cycle. The maximum value of the measured temperature is T_{max}, the minimum value is T_{min}, and the corresponding zonal heating powers are P_{max} and P_{min}, respectively. Considering thermal inertia, when $T_{max}-T_{min}\geq 2℃$, adjust the heating power. After 30 seconds, measure, judge, and adjust the heating power again. The thermal control scheme is shown in Figure 7.

Preprints (www.preprints.org) | NOT PEER-REVIEWED | Posted: 29 December 2023 doi:10.20944/preprints202312.2319.v1

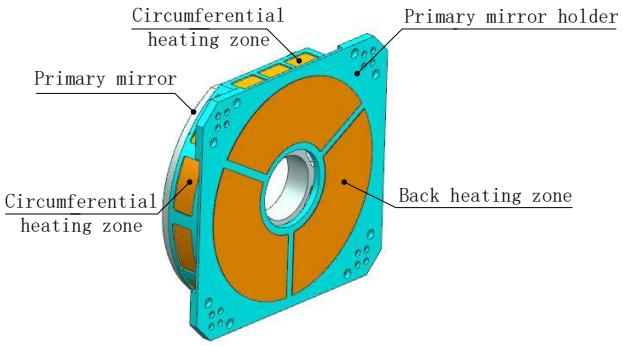

Figure 6. Optimized primary mirror heating.

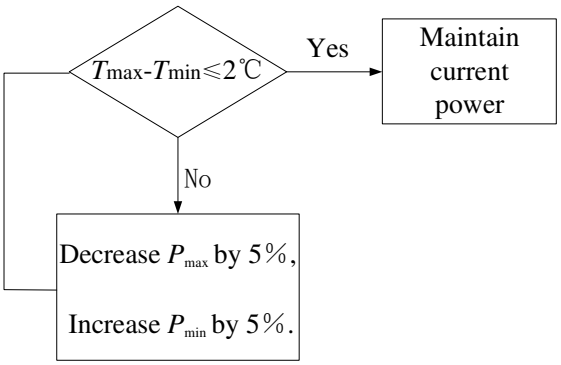

Figure 7. Primary Mirror Thermal Control Scheme.

By conducting the same analysis on the secondary mirror, it was found that due to its smaller size, the convective heat transfer rate Q_{conv}^{sm} on the reflective surface is smaller. Under the same temperature uniformity requirements, the allowable heating power P_{sm} is larger, which is equivalent to Q_{conv}^{sm}. Therefore, heating and temperature measurement are set on the back of the secondary mirror only. To control the temperature difference between the primary mirror and the secondary mirror, a thermal control scheme as shown in Figure 8 is adopted: first, the temperature measured by the primary mirror is averaged as the temperature level T_{pm}; Secondly, compare the difference between the secondary mirror temperature T_{sm} and T_{pm}, and adjust P_{sm} when $|T_{sm} - T_{pm}| \geq 2℃$; Measure the temperature, judge, and adjust P_{sm} again after 30 seconds.

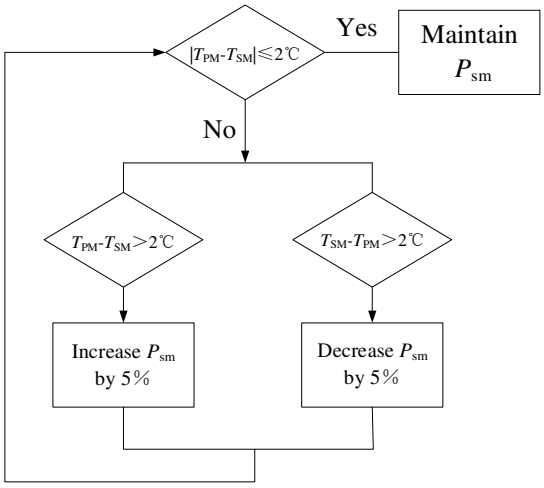

 doi:10.20944/preprints202312.2319.v1

Figure 8. Secondary Mirror Temperature Control Scheme.

4. Test and simulation results

Firstly, heat up the back of the primary mirror and use the optimization scheme proposed in Section 3. Compare the temperature rise and uniformity of different thermal control methods, and compare their numerical results. Secondly, conduct thermal control performance tests on the EO at low temperature to measure temperature and image quality. In 4.1 and 4.2, T_{max} and T_{min} are the measured values of the highest and lowest temperature of the primary mirror respectively; $T_{max\text{-}s}$ and $T_{min\text{-}s}$ are the highest and lowest temperatures of the primary mirror obtained from simulation, respectively. Finally, the thermal control effect under flight conditions is simulated.

4.1. Primary Mirror Heating Test and Simulation

The primary mirror is bonded to the holder and placed vertically. 18 temperature measurement points are arranged on the reflective surface, and 8 temperature measurement points are arranged on the back of the mirror, as shown in Figure 9. When conducting zonal heating, the total power on the back is 24W. On the circumference: 2W for upper part and 4W for lower part. Different heating power P, axial temperature difference ΔT_{ax}, radial temperature difference ΔT_{rad}, average temperature rise ΔT (i.e. the difference between the average temperature of the mirror and the ambient temperature) is shown in Table 1. It should be pointed out that a portion of the heat generated by the heating films undergoes convection with the air, while another undergoes radiation with the environment. The remainder is the effective heating power of the primary mirror. So the values listed in Table 1 are larger than the allowable heating power calculated in Section 3. In addition, due to the vertical position of the mirror, convection will cause the radial temperature difference to be larger than the theoretical value calculated from formula (10). From the results in Table 1, it can be found that back heating method allows only a small P value to ensure temperature uniformity, which leads to a low temperature rise ability of the mirror. By optimized zonal heating, larger power can be used to achieve greater temperature rise while ensuring temperature uniformity. When establishing a thermal analysis model, the heating film is simplified into a two-dimensional sheet, and the heat is evenly distributed in the surface; Features that have a miniscule impact on temperature, such as small holes and small protrusions, have been removed from the model, but the adhesives has been retained and the mesh generation is refined. The measured values and numerical results are shown in Figure 10. The numerical results are relatively close to the measured values, with a maximum error of 1.7℃.

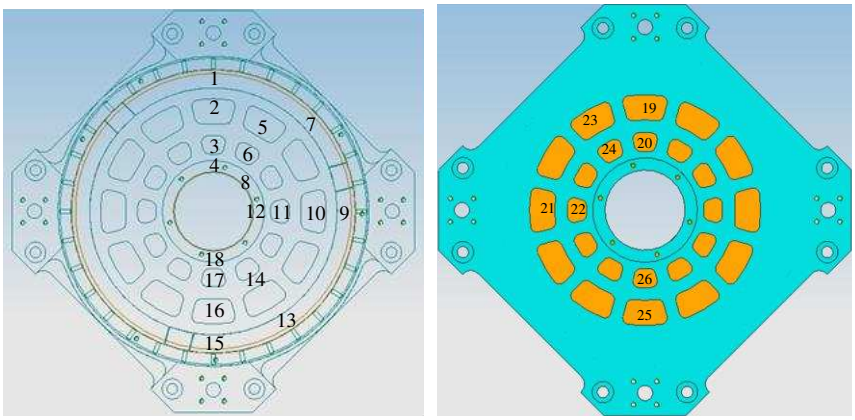

Figure 9. Location of Temperature Measurement Points.

Table 1. Power and Corresponding Temperature.

P/W	Back heating	Optimized zonal heating

Preprints (www.preprints.org) | NOT PEER-REVIEWED | Posted: 29 December 2023 doi:10.20944/preprints202312.2319.v1

	9.6	12.4	23.6	32	30
ΔT_{ax}/℃	1.2	1.4	2.9	3.2	2.5
ΔT_{rad}/℃	2.8	3.7	6.2	7.5	2.1
ΔT/℃	4.3	6.9	9.3	12.9	12.7

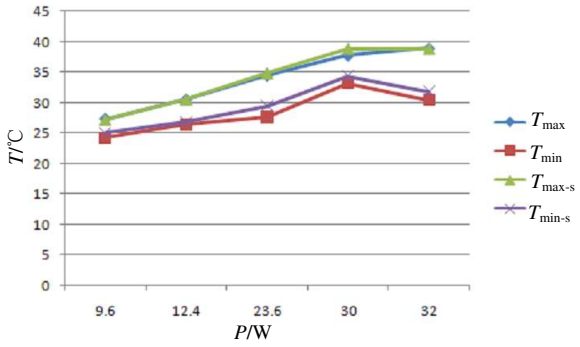

Figure 10. Comparison of measured values and simulation values.

4.2. Low temperature testing and simulation of EO

Apply the optimized thermal control design proposed in the third section to the EO to test T_{pm}, T_{sm}, and image quality at low temperature. The ambient temperature T_{sur} drops from 20℃ to -55℃ within 30 minutes and is kept for 330 minutes. The maximum heating power for the upper part of the shell is 110W, and for the lower part, 130W. To ensure convergence, set the time step increment of the thermal simulation model to 1 second. Due to the fact that the heating of electronic units and imaging sensors has minimal impact on the temperature of the primary mirror and secondary mirror, they are simplified as uniform heat sources without contact with the opto-mechanical structure. This modeling method can save computational resources and ensure accuracy. Due to the frequent rotation during the experiment, the heating power of the primary mirror and secondary mirror is dynamically adjusted with the attitude of EO. The time-temperature curve is shown in Figure 11: the temperature of the primary mirror is uniform, and the difference between the T_{max} and T_{min} does not exceed 5℃. The temperature difference between the primary mirror and the secondary mirror is small; Due to the inability of the model to accurately simulate the rotation and heating power adjustment of the EO, there is a slight error between the numerical results and the test values. Except for $T_{max\text{-}s} - T_{max} = 5.2$℃ at 90 minutes, the maximum deviation of the other values does not exceed 5℃, ensuring satisfied calculation accuracy. The resolution test results at room temperature and low temperature are shown in Figure 12: the resolution at room temperature is 3.43 '', and it cannot be clearly imaged at low temperature without thermal control (as shown in Figure 2). After using optimized thermal control, the resolution at low temperature is 3.82 '', which can effectively ensure image quality.

Preprints (www.preprints.org) | NOT PEER-REVIEWED | Posted: 29 December 2023 doi:10.20944/preprints202312.2319.v1

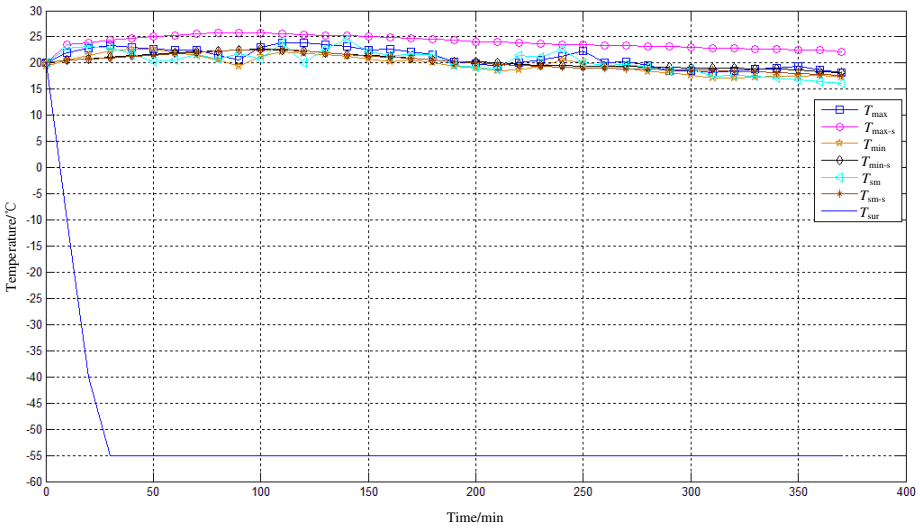

Figure 11. Time-Temperature Curve (Ground Test).

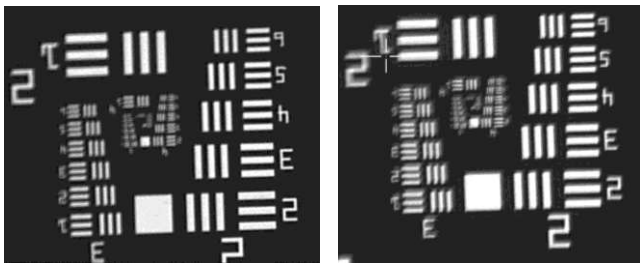

Room temperature Low temperature heating

Figure 12. Resolution test.

4.3. Thermal control simulation under flight conditions

The EO is fixed below the belly of the airplane, where the heat exchange with the external low-temperature environment is complex, and application of the formulas derived from 2 and 3 sections will cause significant errors. Therefore, numerical simulation is used to calculate the temperature of the primary mirror and secondary mirror. The model includes shells, optical window, primary mirror, secondary mirror, primary mirror holder, secondary mirror holder, optic bench, secondary mirror bracket, supporting component, electronic units, imaging sensors, etc. Establish a thermal simulation model using the principles of 4.1 and 4.2, and densified meshes are adopted to discrete the shell, optical window, primary mirror, and secondary mirror, to ensure calculation accuracy, totaling 3672962 nodes. The initial temperature is 20℃, and boundary conditions are set according to the flight speed of 1000km/h and the flight altitude of 20km. The heating power is shown in Table 2. Monitor the temperature at the center of the primary mirror, the lower outer edge, the middle outer edge, the upper outer edge, and the center of the secondary mirror, marked as pm-c, pm-b, pm-m, pm-t, and sm in Figure 13. Figure 13 shows that within 6 hours, the average temperature of the primary mirror is not less than 18℃, its maximum internal temperature difference does not exceed 3℃, and the temperature difference between the primary mirror and the secondary mirror does not exceed 3℃. Combining the results of 4.1 and 4.2, it can be seen that the numerical results have a satisfied confidence level, and corresponding thermal control measures can effectively ensure the image quality.

Preprints (www.preprints.org) | NOT PEER-REVIEWED | Posted: 29 December 2023 doi:10.20944/preprints202312.2319.v1

Table 2. Heating Power.

Position	Shell		Primary mirror		Secondary mirror
	Upper part	Lower part	Back	Circumference	
Power/W	210	240	20	15	5

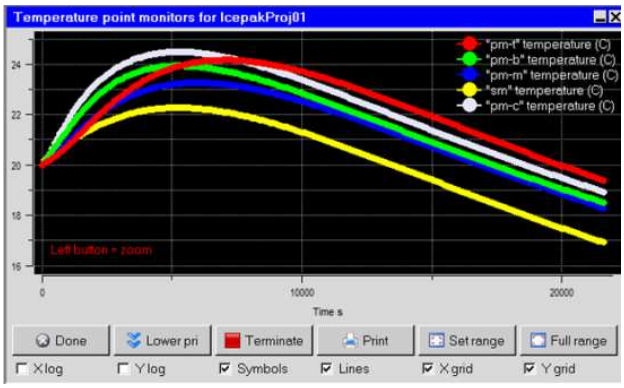

Figure 13. Time-Temperature Curve (Flight Conditions).

5. Conclusion

Through theoretical analysis, temperature and resolution testing, and simulations, the following conclusions are drawn:

1) Large power can be applied on the back of SiC mirror to achieve satisfactory results; Due to the small thermal conductivity of fused silica, it is difficult to balance the temperature uniformity and temperature rise ability of the mirror solely by heating the back only.

2) By arranging heating zones around the circumference in addition to back heating, the temperature uniformity of the fused silica mirror can be effectively ensured, while also having satisfied temperature rise ability, thus ensuring image quality.

3) In practical use, according to changes in environmental temperature and the attitude of the EO, a zonal thermal control design based on temperature negative feedback variable power is adopted to fine tune the power of each heating zone, which can effectively improve the low-temperature environmental adaptability of the EO.

References

1. YU Guobin, LIU Enhai, LIU Guanglin, et al. Moderate resolution imaging camera(MoRIC) of China's first Mars mission Tianwen-1[J]. Earth and Planetary Physics, 2020, 4(4): 364-370.
2. LIU Fuhe, CHENG Zhifeng, JIA Ping, et al. Impact of thermal control measures on the imaging quality of an aerial optoelectronic sensor[J]. Sensors, 2019, 19, 2753.
3. LI Shiqi, WANG Yue, ZHANG Heng, et al. Thermal analysis and validation of GF-4 remote sensing camera[J]. Journal of thermal science, 2020, 29(4): 992-1000.
4. SUN Lu, CHENG Zhifeng, LI Lei, et al. Research on precision thermal control technology based on aerial telefocal common aperture photoelectric platform[J]. Optik- International journal for light and electron optics, 2020, 224.
5. STAHL Philip, KUAN Gary, ARNOLD William, et al. Habitable-Zone explanet observatory baseline 4-m telescope: systems-engineering design process and predicted structural thermal optical performance[J]. Journal of astronomical telescopes, instruments and systems, 2020, 6(3).
6. LEE Junho, JUNG Yongsuk, RYOO Seungyeol, et al. Imaging performance analysis of an EO/IR dual band airborne camera[J]. Journal of the Optical Society of Korea, 2011, 15(2): 174-181.
7. BULERI Christine, YOW Cameryn, CAREY Janak, et al. NASA SAGE SBIR structural, thermal, optical performance(STOP) analysis correlation to wavefront error testing[C]// Proc. of SPIE, 2023,12428.
8. LIU Weiyi, XU Yongsen, YAO Yuan, et al. Relationship analysis between transient thermal control mode and image quality for an aerial camera[J]. Applied optics, 2017, 56(4): 1028-1036.

9. HOLZLOHNER Ronald, KELLERER Aglae, LAMPATER Ulrich, et al. Structural, thermal, and optical performance analysis applied to subsystems of the European extremely large telescope[J]. Journal of astronomical telescopes, instruments and systems, 2022, 8(2).
10. HABER Aleksandar, DRAGANOV John, KRAINAK Michael, Subspace identification of low-dimensional structural-thermal-optical-performance(STOP) models of reflective optics[C]// Proc. of SPIE, 2022,12215.
11. XUE Zhipeng, WANG Chunxue, YU Yue, et al. Integrated optomechanical analyses and experimental verification for a thermal system of an aerial camera[J]. Applied optics, 2019, 58(26): 6996-7005.
12. LI Yanwei, YUAN Guoqin, XIE Xinwang, et al. Multilayer thermal control for high-altitude vertical imaging aerial cameras[J]. Applied optics, 2012, 61(17): 5205-5214.
13. BERGMAN Theodore, LAVINE Adrienne, Fundamentals of heat and mass transfer, 8th edition[M]. Johu Wiley & Sons, Inc., 2017: 549.
14. HOWELL John, MENGUC Pinar, DAUN Kyle, et al. Thermal radiation heat transfer, 7th edition[M]. CRC Press, 2021: 213.
15. YODER Paul Jr, VUKOBRATOVICH Daniel, Opto-mechanical systems design, Fourth Edition, Volume 1: Design and analysis of Opto-mechanical assemblies[M]. Taylor and Francis Group, LLC., 2015.
16. CHENG Zhifeng, SUN Lu, LIU Fuhe, et al. Engineering design of an active-passive combined thermal control technology for an aerial optoelectronic platform[J]. Sensors, 2019, 19, 5241.